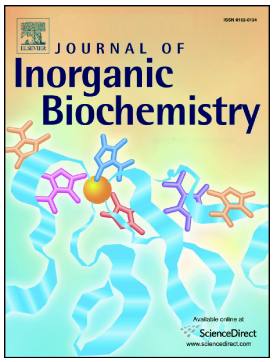

Half-sandwich IridiumIII N-heterocyclic carbene antitumor complexes and biological applications

Yali Han, Zhenzhen Tian, Shumiao Zhang, Xicheng Liu, Juanjuan Li, Yanru Li, Yi Liu, Min Gao, Zhe Liu

PII: S0162-0134(18)30458-6
DOI: doi:10.1016/j.jinorgbio.2018.09.009
Reference: JIB 10564

To appear in: *Journal of Inorganic Biochemistry*

Received date: 31 July 2018
Revised date: 10 September 2018
Accepted date: 11 September 2018

Please cite this article as: Yali Han, Zhenzhen Tian, Shumiao Zhang, Xicheng Liu, Juanjuan Li, Yanru Li, Yi Liu, Min Gao, Zhe Liu , Half-sandwich IridiumIII N-heterocyclic carbene antitumor complexes and biological applications. Jib (2018), doi:10.1016/j.jinorgbio.2018.09.009

Half-sandwich Iridium^{III} *N*-heterocyclic Carbene Antitumor Complexes and Biological Applications

Yali Han, Zhenzhen Tian, Shumiao Zhang, Xicheng Liu, Juanjuan Li, Yanru Li, Yi Liu, Min Gao, Zhe Liu**

Institute of Anticancer Agents Development and Theranostic Application, The Key Laboratory of Life-Organic Analysis and Key Laboratory of Pharmaceutical Intermediates and Analysis of Natural Medicine, School of Chemistry and Chemical Engineering, Qufu Normal University, Qufu 273165, China.

**Corresponding author (Email): chemlxc@163.com (X.C. Liu); liuzheqd@163.com (Z. Liu)*

Abstract

Series of half-sandwich Ir^{III} *N*-heterocyclic carbene (NHC) antitumor complexes [(η^5-Cp*)Ir(C^C)Cl] have been synthesized and characterized (Cp* is pentamethyl cyclopentadienyl, and C^C are four NHC chelating ligands containing phenyl rings at different positions). Ir^{III} complexes showed potent antitumor activity with IC_{50} values ranged from 3.9 to 11.8 μM against A549 cells by the MTT assay. Complexes can catalyze the conversion of the coenzyme NADH to NAD^+ and induce the production of reactive oxygen species (ROS), and bonding to BSA by static quenching mode. Complexes can arrest the cell cycle in G_1 or S phase and reduce the mitochondrial membrane potential. Confocal microscopy test show complexes could target the lysosome and mitochondria in cells with the Pearson's colocalization coefficient of 0.82 and 0.21 after 12 h, respectively, and followed by an energy-dependent cellular uptake mechanism.

Key words: Half-sandwich; Iridium^{III} complex; *N*-heterocyclic carbene; Antitumor

1. Introduction

Cancer is threatening people's health, and the research on anticancer drugs has caused widespread concern. Anticancer drugs mainly include natural drugs and chemical synthetic drugs [1, 2], among these, metal-centered platinum antitumor drugs are most widely used in clinical practice. Although cisplatin and its derivatives have achieved great success in clinical applications, the development of which is hindered by many drawbacks, e.g., serious side-effects and easily acquired drug

resistance [3-6]. Even so, the successful clinical application of platinum drugs has promoted the research process of other metal antitumor drugs [7]. Recently, non-platinum-based compounds such as iridium complexes are attracting more and more attention [8, 9], and which have significant potential to become alternatives to platinum-based metal anticancer agents [10, 11].

Iridium antitumor complexes mainly include two types: half-sandwich and cyclometalated iridium complexes. Due to the higher antitumor activity, half-sandwich Ir^{III} complexes have attracted considerable attention. The general form of half-sandwich Ir^{III} complexes can be expressed as $[(Cp^x)Ir(L\text{^}L)Z]$, Cp^x represents the electron-rich cyclopentadienyl group and its derivatives, Z is the leaving group, and L^L is chelating ligand. Previous study showed the introduction of electron-rich Cp* in Ir^{III} complexes can increase the stability of ligand binding to metal iridium [12-14]. And also, the type and the size of chelating ligands could obviously influence the targeted sites, the lipid solubility and even antitumor activity for half-sandwich Ir^{III} complexes.

N-heterocyclic carbene (NHC) metal complexes have been extensively used in various fields, especially as potential anticancer agents [15-17]. Previous study showed cyclic double carbene ligands Ir^{III} complexes directly activate the mitochondrial energy production system of cancer cells, generating reactive oxygen species (ROS) and activating mitochondria-dependent cell death signaling pathways [18-20]. However, the study of half-sandwich Ir^{III} NHC complex applied to antitumor field was rare [21, 22]. In this study, four half-sandwich Ir^{III} NHC complexes of the type [(Cp*)Ir(C^C)Cl] (Complexes **1-4**, Scheme 1) were synthesized and characterized. Cp* is pentamethylcyclopentadienyl, C^C are four diverse NHC chelating ligands containing phenyl rings at different positions [23]. As-synthesized Ir^{III} complexes displayed a favorable antitumor activity against A549 lung cancer cells (IC_{50}: 3.9-11.8 μm) than cisplatin (21.3 μm) under the same conditions. Complexes were able to bind with bovine serum albumin (BSA) and oxidize NADH (nicotinamide adenine dinucleotide) to NAD^+, which inducing the production of reactive oxygen species (ROS) [24, 25]. Complexes can arrest the cell cycle and

induce apoptosis. Confocal microscopy test show complexes could target the lysosome and mitochondria in cells with the Pearson's colocalization coefficient of 0.82 and 0.21 after 12 h, respectively, and followed by an energy-dependent cellular uptake mechanism [26-28]. The results suggest that half-sandwich Ir^{III} NHC complexes are hopeful for development as new antitumor agents.

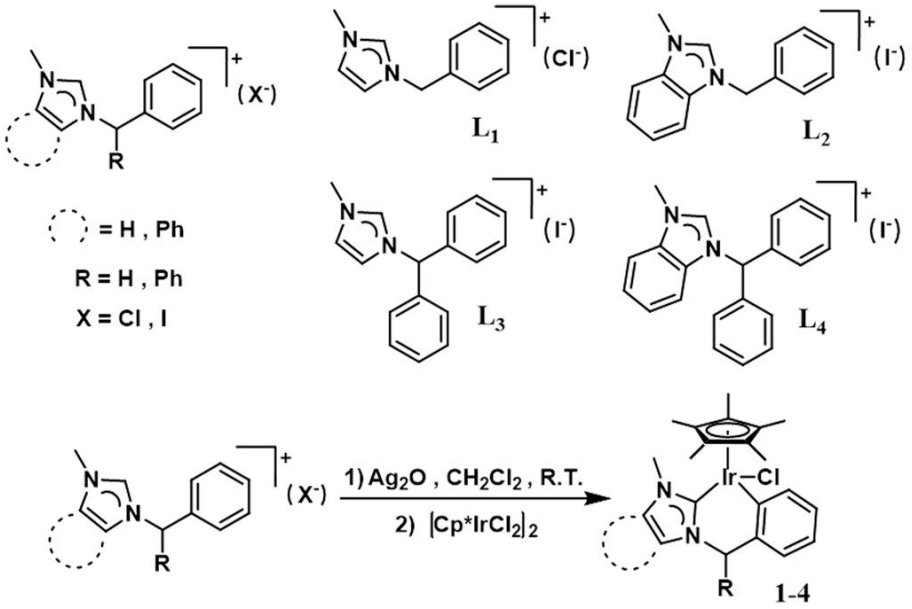

Scheme 1. The selcted NHC chelating ligands (**L_1-L_4**) and the synthetic process of Ir^{III} NHC complexes **(1-4).**

2. Results and Discussion

2.1 Synthesis and Characterization

Half-sandwich Ir^{III} NHC complexes of the type [(Cp*)Ir(C^C)Cl] were synthesized in dichloromethane at ambient temperature using silver oxide (Ag_2O) catalyzed reaction. NHC chelating ligands were obtained by the reaction of the corresponding imidazole and iodine hydrocarbon. All of Ir^{III} NHC complexes were newly synthesized complexes and achieved in good yields. The synthetic processes are shown in Scheme 1. Ir^{III} NHC complexes and the intermediates were marked by nuclear magnetic resonance spectrum (^{1}H NMR), mass spectroscopy (MS) and elemental analysis. Complexes were non-hygroscopic and highly soluble in common organic solvents such as dichloromethane, chloroform, dimethyl sulfoxide, partially dissolved in methanol, insoluble in ether, hexane and petroleum ether.

2.2 Cytotoxicity Test

The antitumor activity of Ir^{III} NHC complexes against A549 human lung cancer cells was determined by the MTT assay [29-31]. As shown in Table 1, all complexes showed better antitumor activity than cisplatin (widely used in clinical practice), with the IC_{50} values ranged from 3.9 to 11.8 μM. Compared with complex **1**, complexes **2-4** have the better antitumor activity, which is mainly due to the enhanced lipid solubility caused by the introduction of more phenyl to NHC chelating ligands. The log P (partition coefficient in oil/water) for complexes **1** and **4** were determined by inductively coupled plasma mass spectrometry (ICP-MS), the values were -1.12 and -0.57, respectively. The data show that the increase of the benzene ring to NHC chelating ligands can effectively increase the lipid solubility of the complex. However, the position and number of benzene rings have little change in the activity of complexes **2-4**. In order to further study the antitumor mechanism of Ir^{III} NHC complexes, complexes **2** and **3** were selected as representatives, and further studied.

Table 1. IC_{50} values of complexes **1-4** and cisplatin against A549 cells determined by MTT assay after 24 h.

Complex	IC_{50} (μM)
$[(\eta^5\text{-}C_5Me_5)Ir(\mathbf{L_1})Cl]$ (**1**)	11.8±1.2
$[(\eta^5\text{-}C_5Me_5)Ir(\mathbf{L_2})Cl]$ (**2**)	5.9±0.4
$[(\eta^5\text{-}C_5Me_5)Ir(\mathbf{L_3})Cl]$ (**3**)	4.6±0.2
$[(\eta^5\text{-}C_5Me_5)Ir(\mathbf{L_4})Cl]$ (**4**)	3.9±0.7
Cisplatin	21.3±1.7

2.3 Reaction with NADH

NADH and NAD^+ are indispensable substances in various bio-catalytic reactions. [32]. NADH can contribute hydride to transition metal-based complex and promote the production of ROS (H_2O_2), thus serving as a pathway for the oxidation mechanism [33]. Interaction between Ir^{III} NHC complexes and NADH was determined by ultraviolet-visible (UV-Vis) spectrum. The maximum absorbance of NADH and NAD^+ can be determined in 339 and 259 nm, respectively. As shown in Fig. 1A (Fig.

S1, ESI), with the increase of complexes, the absorption of 339 nm showed a significantly reduced and an increase in 259 nm which further confirmed the catalytic activity of Ir^{III} NHC complexes [33]. The turn over numbers (TONs) values of complexes **2** and **3** were shown in Fig. 2B. As shown, complex **3** had the bigger TONs value, which was correspond with the result of MTT assay. The bigger of the TONs value, the better of antitumor activity.

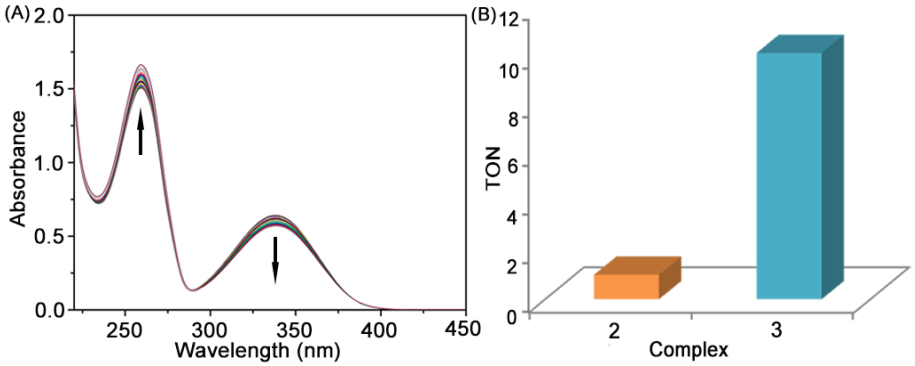

Fig. 1 (A) Reaction of complex **3** (1.0 μM) and NADH (100 μM) in a 60% MeOH/40% H_2O (v/v) mixed solution was monitored by UV-Vis at 298 K over 8 h. (B) The TONs of complexes **2** and **3**.

2.4 Protein interaction

Serum albumin (SA) has the highest abundance in plasma and excellent binding properties, so it is typically used in the delivery of drugs in the blood system [34-37]. As a kind of transport protein, bovine serum albumin (BSA) has the advantages of cheap, stable, easy to purify and similar to human serum albumin (HSA) [38], which was chose as a model to study the interaction between complexes and proteins.

The UV-Vis absorption spectrum of BSA in the presence of complexes **2** and **3** are shown in Fig. 2 and Fig. S2, ESI. The internal filtration effect can be eliminated by UV-Vis and aim at further fluorescence intensity studies. With the increase of complexes, the maximum absorption at 228 nm decreased, which is mainly due to the induced perturbation of BSA because of Ir^{III} compounds. [39-41]. Obvious red-shift was found at 228 nm attribute to the effect of the polar solvent (water). However, there is no obvious shift in 278 nm, which indicated the microenvironment of the three aromatic acid residues in BSA (Trp, Tyr and Phe) was changed because of Ir^{III}

NHC complexes [42].

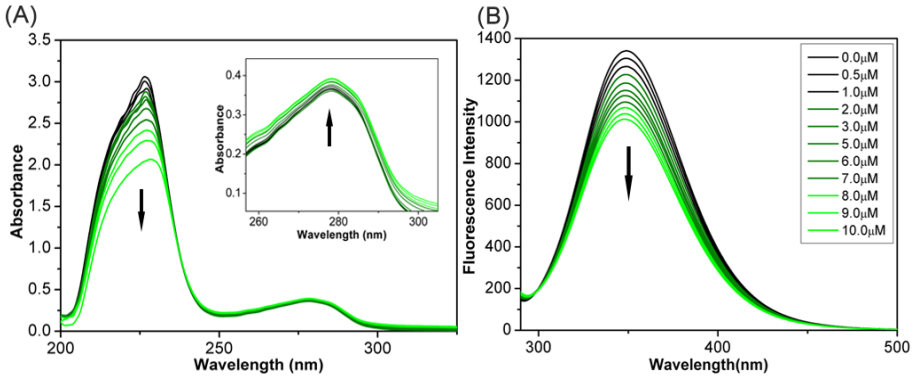

Fig. 2 (A) Complex **3** was increased from 0 μM to 10 μM, UV-Vis spectra of BSA in Tris-HCl/NaCl buffer solution (pH=7.2). Arrows indicate the direction of change in absorbance as the concentration of the complex increases. Inset: Wavelength absorbance changes from 200 to 320 nm. (B) The complex **3** was increased from 0 μM to 10 μM, and the fluorescence spectrum of BSA was changed (0.5 μM, λ_{ex}=280 nm, λ_{em}=343 nm).

The fluorescence emission spectra of BSA with different concentrations of complexes **2** and **3** at 298 K are presented in Fig. 2B and Fig. S2B, ESI. As shown, fluorescence intensity of BSA quenched obviously with the increase of complexes. The quenching rate constant K_q and Stern–Volmer quenching constant K_{sv} were calculated by classical Stern-Volmer equation (Fig. S3, ESI), and the binding constant K_b and binding site number **n** of complexes were obtianed by the Scatchard equation (Fig. S4, ESI) [43]. As shown in Table 3, the values of K_q for complexes **2** and **3** were 3.92×10^{12} and 3.21×10^{12} M^{-1} s^{-1}, which are about two orders of magnitude higher than that of a pure dynamic quenching mechanism (2.0×10^{10} M^{-1} s^{-1}) [44]. These indicated that the interaction between Ir^{III} NHC complexes and BSA have been followed by a static quenching mechanism dominates. The binding site number (**n**) was almost the same (~1), but complex **3** having a slightly larger binding constant (K_b) values than complex **2**, which was consistent with the conclusion that complex **3** had the higher antitumor activity.

Table 3. Quenching parameters and binding parameters for the interaction of the complex **2** and complex **3** with BSA.

Complex	K_{sv} ($10^4 M^{-1}$)	K_q ($10^{12} M^{-1}s^{-1}$)	K_b ($10^4 M^{-1}$)	n
2	3.92±0.73	3.92	2.06	1.29
3	3.21±0.29	3.21	2.55	1.14

Information on tyrosine residues and tryptophan residues in the BSA microenvironment can be displayed at the same fluorescence spectra $\Delta\lambda$ = 15 nm and $\Delta\lambda$ = 60 nm [45]. As shown in Figs. S5-S6, ESI, the fluorescence intensity at 291 nm and 285 nm ($\Delta\lambda$ = 15 nm and 60 nm), which are the characteristic of the synchronous emission spectra for tyrosine and tryptophan residues of BSA, reduced with the increase of compounds **2** and **3**. At $\Delta\lambda$ = 15 nm, a slight blue shift of 2 nm was observed in the complex **3** (Fig. S6), and a slight red shift of 3 nm was observed for complex **2** at $\Delta\lambda$ = 60 nm. The above results clearly shows that Ir^{III} NHC complexes could act on BSA by affecting its microenvironment.

2.5 Cell cycle analysis

As shown in Fig. 3 (Fig S7, Table S1 and S2, ESI), the cell cycle arrest for A549 cells exposure to complexes **2** and **3** with the concentrations of 0.25, 0.5 and 1.0×IC_{50} for 24 h have been determined by flow cytometry. At a concentration of 2.0×IC_{50}, the percentages of cells in the Sub-G_1 phase increased from 58.1% to 64.7% when exposure to complex **2**, which indicating cells failed to synthesize RNA and protein normally, or affecting the energy supply to the next stage of the cell [31, 35]. For complex **3**, the percentages of cells in the S phase increased 7.8%, which indicating complex **3** may block the synthesis of DNA and histone, or some DNA replication-related enzymes [35]. Compared with the untreated control, the cell cycle was disturbed in sub-G_1 and S phase for complexes **2** and **3**, respectively. The results indicate that Ir^{III} NHC complexes can disturb the cell growth cycle progression, and achieving the objective of apoptosis.

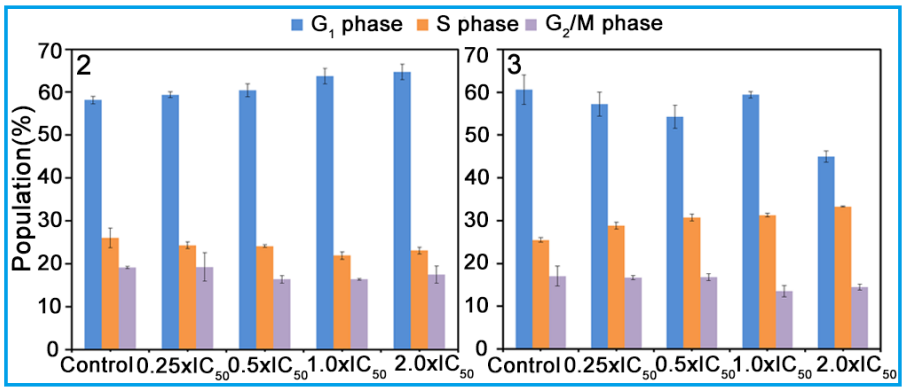

Fig. 3 Histogram data of cell cycle distribution of A549 cancer cells of complexes **2** and **3** after 24 h. Tests were performed using 0.25, 0.5, 1.0, and 2.0 times of the IC_{50} equivalent concentration. The data is taken as mean ± SD of three measurements. Cell staining for flow cytometry was carried out using PI/RNase.

2.6 Induction of apoptosis

To determine whether cell function decline was associated with apoptosis, A549 cells were treated with complexes **2** and **3** at 1.0, 2.0, and 3.0 equivalents IC_{50} for 24 hours. After staining with Annexin, data were measured by flow cytometry [46]. As shown in Fig. 4 and Tables S3- S4, ESI, the population of the early and late apoptotic phase had a significant increase with the value ranged from 1.0% and 4.3% to 2.1% and 29.8% after 24 h, respectively, when the concentration changed from $1.0\times IC_{50}$ to $3.0\times IC_{50}$ for complex **2**. For complex **3** (Fig. 4), about 39.0% of the A549 cells were undergoing apoptosis, including 32.0% of cells in the late apoptosis, while 95.8% of untreated cells are still alive under the same conditions.

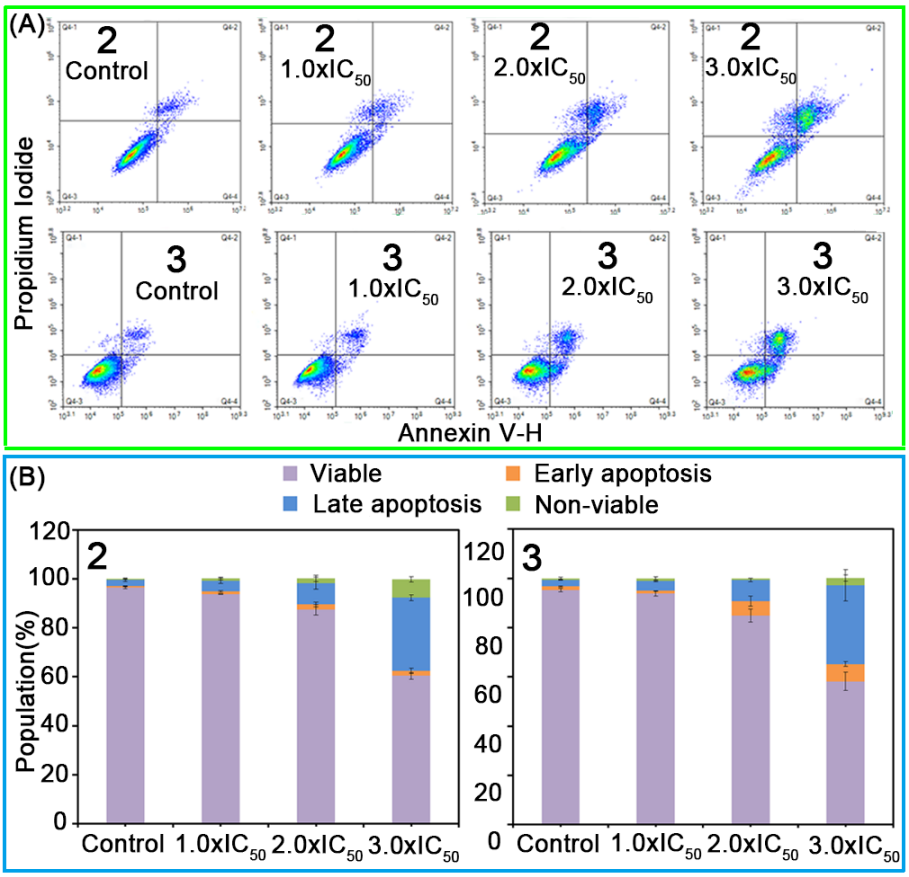

Fig. 4 (A) Apoptosis analysis of A549 cancer cells after 24 h of exposure to complexes **2** and **3** at 310 K determined by flow cytometry with Annexin V-FITC vs PI staining. (B) Histogram showing populations for A549 cells in four stages treated by complexes **2** and **3**. Data are quoted as mean ± SD of three replicates.

2.7 Induction of ROS

The accumulation of ROS produced in mitochondrial will lead to apoptosis, which can be used to explore the function mechanism of antitumor agents. By means of flow cytometry, the level of ROS was determined in A549 cells for complexes **2** and **3** after 24 h. As shown in Fig. 5 and Tables S5-S6, ESI, compared with the control, the level of ROS increased by 1.3 and 1.4 times for complex **2** in the concentration of $0.25\times IC_{50}$ and $0.50\times IC_{50}$, respectively. For complex **3**, the level of ROS only increased by 1.1 times with the concentration of $0.5\times IC_{50}$. The results indicate that Ir^{III} NHC complexes could induce the production of ROS, which provide a basis that complexes could affect the mitochondria and lead to apoptosis.

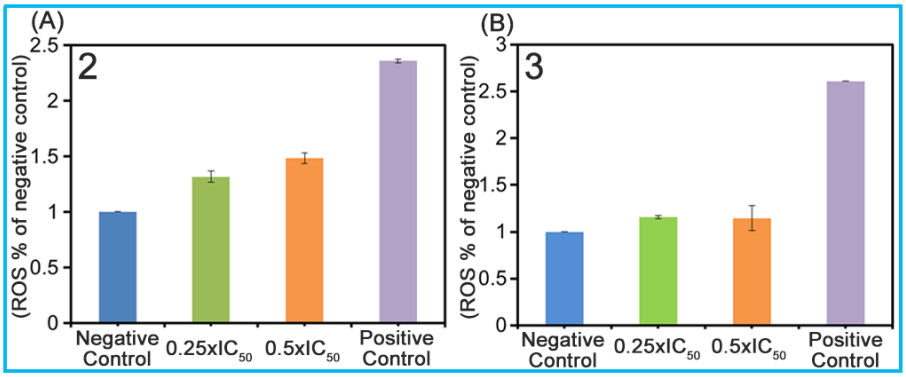

Fig. 5 A549 cancer cells were incubated with complexes **2** (A) and **3** (B) at concentrations of $0.25\times IC_{50}$ and $0.5\times IC_{50}$ to induce ROS production. Taking the ROS level of negative control as the standard to make the histogram.

2.8 Mitochondrial membrane potential

Mitochondrial dysfunction may be involved in the cause of cell death [47-49]. The extent of mitochondrial dysfunction can be assessed by the loss of the mitochondrial membrane potential (MMP). As shown in Fig. 6, Fig. S8 and Tables S7-S8, ESI, the loss of MMP induced by complexes **2** and **3** was assessed by detecting the JC-1 dye (the decrease in red fluorescence and increased green fluorescence) using flow cytometry. At the indicated concentrations, a significant concentration-dependent increase was found with a remarkable loss of MMP, e.g. from 34.3% and 7.8% (control) to 60.1% and 30.6% ($2.0\times$ IC_{50}) for complexes **2** and **3**, respectively, which proving Ir^{III} NHC complexes could act on mitochondria and induce apoptosis.

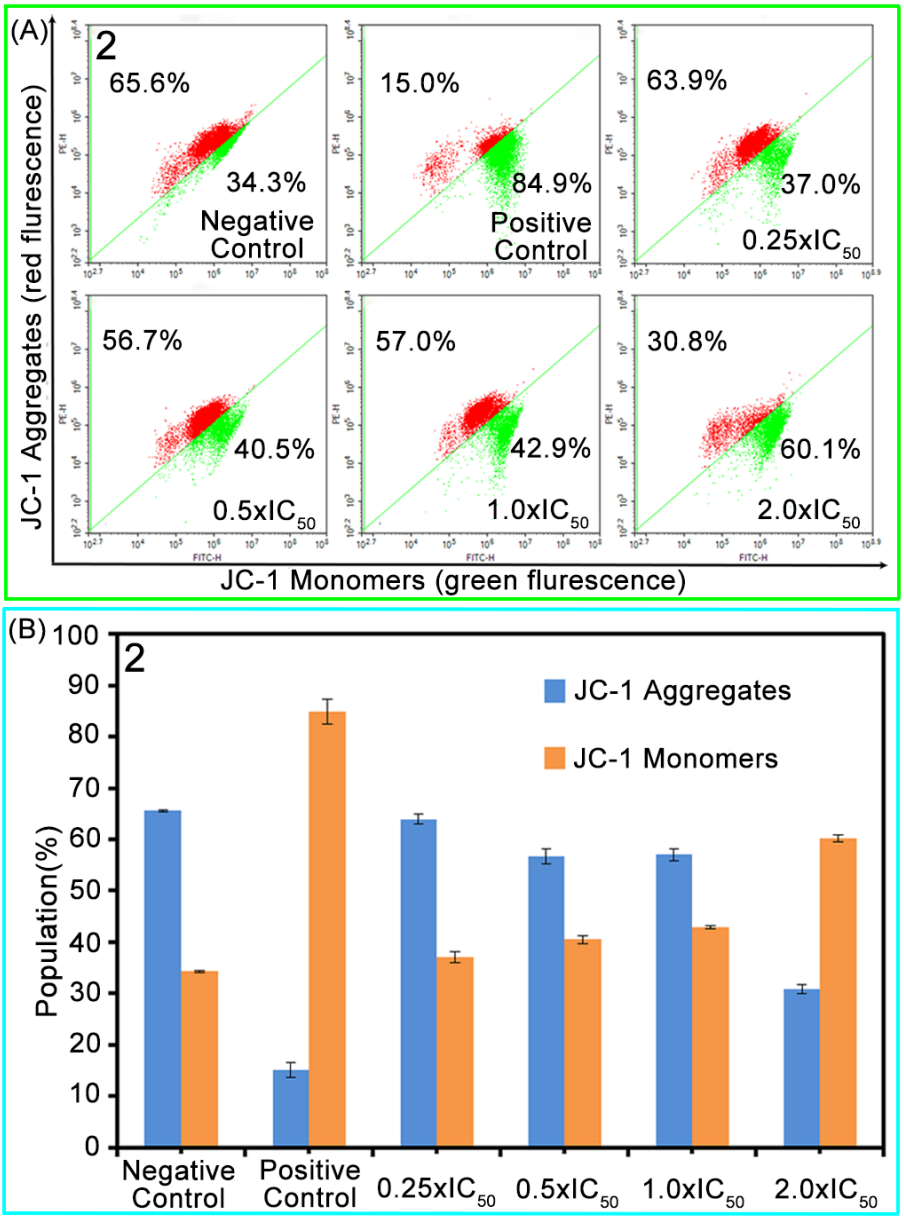

Fig. 6 (A) At concentration of 0.25×IC_{50}, 0.5×IC_{50}, 1.0×IC_{50} and 2.0×IC_{50}, the loss of MMP induced by complex **2** using JC-1 dye. The red aggregates and green monomers are gated. (B) Histograms for the MMP treated with different concentrations of complex **2**. The above data is the average ± SD of three measurements repeated.

2.9 Cell imaging and cellular uptake

Subcellular localization of complexes **2** and **3** can be easily determined by laser confocal microscopy in A549 cells on account of their intrinsic luminescence. The Lyso Tracker Red DND-99 (LTRD) and Mito Tracker Deep Red (MTDR) were used as lysosomes and mitochondria fluorescence probes, respectively. As shown in Fig. 7

(Fig. S9, ESI), selected representative complex **3** could effectively target lysosomes with the Pearson coefficients of 0.75, 0.88, and 0.82 when incubated for 1, 6 and 12 h, respectively. In addition, complex **3** could also target mitochondria with the Pearson coefficients of 0.21, 0.17, and 0.23 after 1, 6 and 12 h, respectively, although it was not apparent. And also, the complex did not immediately lead to abnormal cell death, enabling us to track changes in lysosome morphology in real time [6].

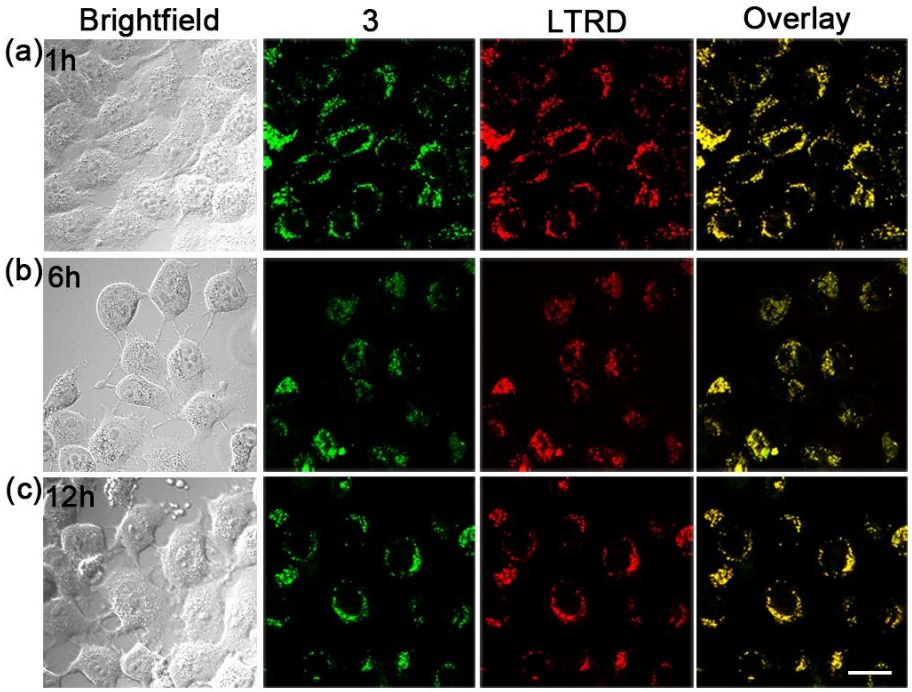

Fig. 7 Confocal microscopic images of A549 cells co-labeled with complex **3** (10 μM, 1h, 6h, 12h) and LTRD (75 nM, 1h). Complex **3** and LTRD were excited at 488 nm and 594 nm, respectively. Complex **3** collects fluorescence in 549-651nm and LTRD collects fluorescence in 493-630nm. Scale bar: 20 μm.

Lysosomal permeability is often triggered by the disruption of the lysosomal integrity [50]. To investigate whether lysosomal damage induced by complex **3** was accompanied by lysosome targeting specificity. Lysosomal integrity of A549 cells were evaluated by acridine orange (AO) staining after treatment with **3** for 6 h with the concentration of 1.0 × IC_{50} and 3.0 × IC_{50} [51, 52]. AO exhibits red fluorescence when accumulated in lysosome and green fluorescence when bounding to RNAs in

the nuclei or cytosol. As shown in Fig. 8, compared with control, red fluorescence basically disappears in lysosome when exposed to complex **3** (1.0 × IC_{50}) after 6 h, and obvious lysosomal damage was found at 3.0 × IC_{50}.

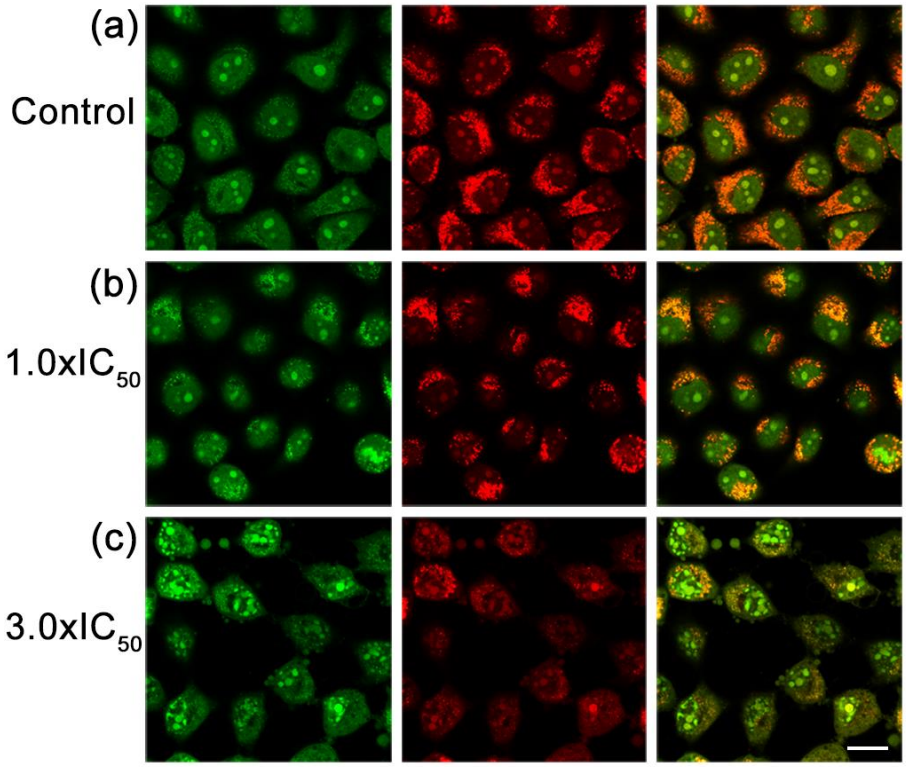

Fig. 8 AO-loaded A549 cells (a) as a control group, no drug was added to the cells. (b) After addition of complex **3** (1.0 × IC_{50}) for 6 h, AO (5 μM) was added for 15 min after laser confocal detection. (c) After addition of complex **3** (3.0 × IC_{50}) for 6 h, AO (5 μM) was added for 15 min after laser confocal detection. Complex **3** was excited at 488 nm and collected at a wavelength of 493-630 nm. Scale bar: 20 μm.

Drug molecules can enter cells with different transport mechanisms, including energy-dependent mechanisms (such as endocytosis and active transport) and energy-independent mechanisms (such as diffusion-promoting and passive diffusion) [53]. Therefore, carbonyl cyanide *m*-chlorophenylhydrazone (CCCP) and chloroquine were used as energy inhibitor and endocytic inhibitor to study the mechanism of cellular uptake, respectively. The cells incubated at 277 K and 310 K for 2 h and then pretreatment with CCCP and chloroquine. As shown in Fig. 9, the uptake of cells

reduced efficiency after incubated at 273 K, which suggested that cellular uptake of complex **3** was followed by an energy-dependent mechanism.

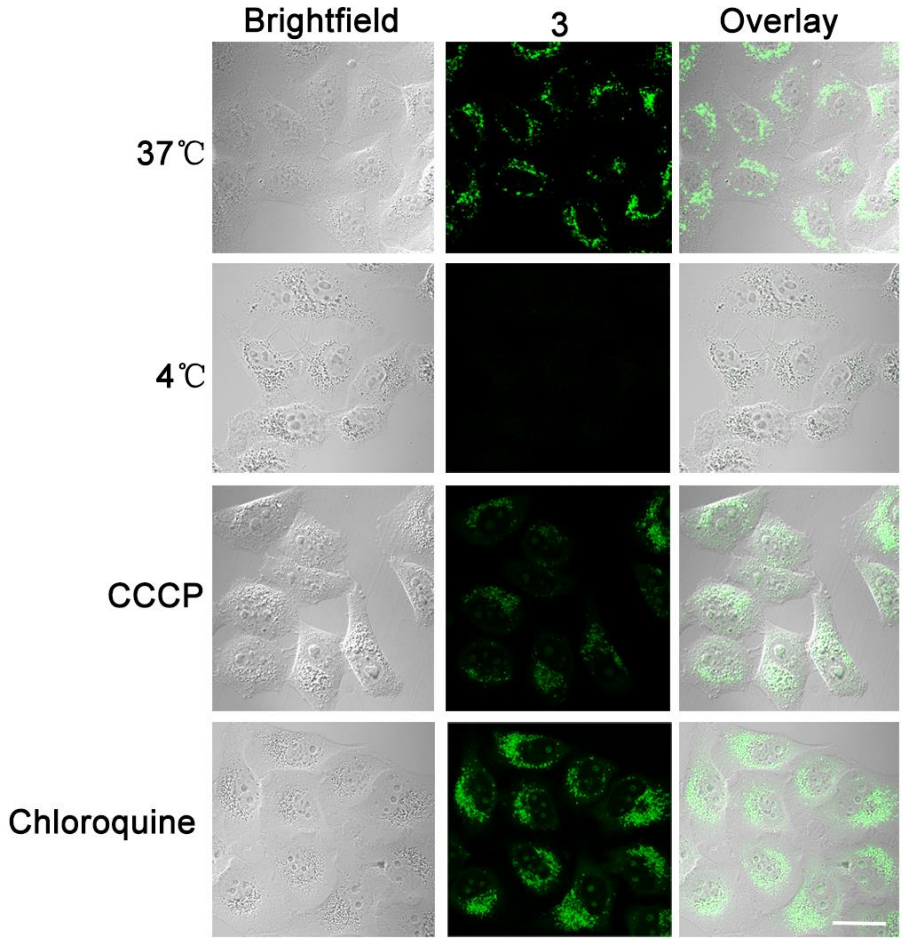

Fig. 9 Effect of incubation temperature (37 ºC and 4 ºC), metabolic inhibitor (CCCP, 50 μM) and chloroquine (50 μM) on cellular uptake of **3** (10 μM, 30 min) measured by confocal microscopy. Complex **3** was excited at 488 nm and emission was collected at 493-630 nm. Scale bar: 20 μm.

3. Conclusions

In this study, four new half-sandwich Ir^{III} NHC complexes were synthesized with simple synthetic procedures. All complexes showed favorable antiproliferative activity. Complex **4** showed the best activity towards A549 lung cancer cells, which were five times higher than the clinical antitumor drug cisplatin. Complexes can effectively bind with BSA, catalyzing NADH to NAD^+ and inducing ROS, which will disturb the cell growth cycle and lead to apoptosis. Complexes can specifically target lysosomes and mitochondria, entering cells through energy-dependent mechanisms,

and destroying the integrity of lysosomes. Above all, half-sandwich Ir^{III} NHC complexes could be a promising candidate for further evaluation as antitumor drugs.

4. Experimental section

1H-imidazole, 1H-benzimidazole, 1-benzyl-3-methylimidazoliumiodide (**L_1**), 1-benzylbenzimidazole, 1-diphenylmethylimidazole, 1-(diphenylmethyl) -1H-benzimidazole and the dimer $[Cp^*IrCl_2]_2$ were prepared according to literature procedures [54]. All other reagents are used as supplied by the commercial supplier. Nitrogen was used as the drying and filling gas.

*Synthesis of **L_2-L_4.***

1-benzylbenzimidazole (2.5 g, 12 mmol) was dissolved in 10 mL of acetonitrile, and then iodomethane (1.1 mL, 18 mmol) were added. The mixture was refluxed overnight. After rotary evaporation, yellow oil product was washed with diethyl ether, pure yellow salt was obtained. Yield: 2.2 g (86%). ^{1}H NMR (500 MHz, $CDCl_3$) δ 11.23 (s, 1H), 7.71 (d, *J* = 8.3 Hz, 1H), 7.65 (s, 1H), 7.60 (s, 2H), 7.53 (d, *J* = 6.4 Hz, 2H), 7.39 (d, *J* = 7.3 Hz, 3H), 5.83 (s, 2H), 4.28 (s, 3H).

L_3 and **L_4** were synthesized using the same method, the representation data is as follows:

L_3: Yield: 79%. ^{1}H NMR (500 MHz, $CDCl_3$) δ 9.67 (s, 1H), 7.43 (s, 2H), 7.41 (s, 5H), 7.33 – 7.30 (m, 5H), 7.08 (s, 1H), 4.08 (s, 3H).

L_4: Yield: 74%. ^{1}H NMR (500 MHz, $CDCl_3$) δ 10.21 (s, 1H), 7.71 (d, *J* = 8.3 Hz, 1H), 7.64 (d, *J* = 7.6 Hz, 1H), 7.50 (d, *J* = 7.7 Hz, 1H), 7.45 (s, 10H), 7.29 (s, 1H), 7.20 (s, 1H), 4.31 (s, 3H).

*Synthesis of the complexes **1–4.***

In a round bottom flask, silver oxide (2.4 eq) and chelating ligands (**L_1-L_4**) (2.0 eq) were added to a solution of dichloromethane (CH_2Cl_2). After 8 h, the mixture was filtered through Celite and washed with CH_2Cl_2. The combined filtrates were added dropwise to a solution of CH_2Cl_2 containing $[Cp^*IrCl_2]_2$ (1.0 eq). The mixture was stirred at room temperature for another 8h and filtered through Celite. The solvent was removed in vacuum， and the product was recrystallized from CH_2Cl_2 / n-hexane to give a pure yellow product. Detailed characterization data of complexes **1–4** were

as follows:

[(η^5-C_5Me_5)Ir(**L_1**)Cl] (**1**): Yield: 79%. ^{1}H NMR (500 MHz, $CDCl_3$) δ 7.62 (d, *J* = 7.5 Hz, 1H), 6.97 (dd, *J* = 12.9, 7.0 Hz, 2H), 6.94 (d, *J* = 2.0 Hz, 1H), 6.90 (d, *J* = 1.9 Hz, 1H), 6.81 (t, *J* = 7.3 Hz, 1H), 4.86 (d, *J* = 13.8 Hz, 1H), 4.65 (d, *J* = 13.9 Hz, 1H), 3.93 (s, 3H), 1.68 (s, 15H). Elemental analysis: Found: C, 50.49; H, 5.21; N, 5.64%, calcd for $C_{21}H_{26}ClIrN_2$: C, 50.58; H, 5.26; N, 5.62%. ESI-MS (*m/z*): calcd for $C_{21}H_{26}IrN_2$: 498.67 $[M\text{-}Cl]^+$; found 499.42.

[(η^5-C_5Me_5)Ir(**L_2**)Cl] (**2**): Yield: 72%. ^{1}H NMR (500 MHz, $CDCl_3$) δ 7.87 (d, *J* = 7.6 Hz, 1H), 7.46 (d, *J* = 7.7 Hz, 1H), 7.34 (d, *J* = 7.7 Hz, 1H), 7.28 (d, *J* = 6.7 Hz, 1H), 7.23 (d, *J* = 7.4 Hz, 1H), 7.08 – 7.05 (m, 1H), 6.92 (t, *J* = 7.4 Hz, 1H), 6.81 (t, *J* = 7.0 Hz, 1H), 5.16 (d, *J* = 14.2 Hz, 1H), 5.03 (d, *J* = 14.1 Hz, 1H), 4.04 (s, 3H), 1.82 (s, 15H). Elemental analysis: Found: C, 50.78; H, 5.10; N, 5.09%, calcd for $C_{25}H_{28}ClIrN_2$: C, 50.72; H, 5.14; N, 5.11%. ESI-MS (*m/z*): calcd for $C_{25}H_{28}IrN_2$: 548.73 $[M\text{-}Cl]^+$; found 549.33.

[(η^5-C_5Me_5)Ir(**L_3**)Cl] (**3**): Yield: 74%. ^{1}H NMR (500 MHz, $CDCl_3$) δ 7.97 (d, *J* = 7.6 Hz, 1H), 7.51 (d, *J* = 6.7 Hz, 3H), 7.44 (s, 2H), 6.84 (t, *J* = 7.1 Hz, 1H), 6.80 (s, 1H), 6.61 (t, *J* = 7.4 Hz, 1H), 6.38 (d, *J* = 8.7 Hz, 2H), 5.98 (s, 1H), 3.90 (s, 3H), 1.81 (s, 15H). Elemental analysis: Found: C, 52.49; H, 5.23; N, 4.35%, calcd for $C_{27}H_{30}ClIrN_2$: C, 53.06; H, 5.11; N, 4.28%. ESI-MS (*m/z*): calcd for $C_{27}H_{30}IrN_2$: 574.77 $[M\text{-}Cl]^+$; found 575.33.

[(η^5-C_5Me_5)Ir(**L_4**)Cl] (**4**): Yield: 68%. ^{1}H NMR (500 MHz, $CDCl_3$) δ 7.95 (d, *J* = 7.7 Hz, 1H), 7.53 (s, 1H), 7.46 (d, *J* = 6.5 Hz, 4H), 7.09 – 7.04 (m, 2H), 6.84 (t, *J* = 7.5 Hz, 1H), 6.70 (t, *J* = 7.4 Hz, 1H), 6.61 (t, *J* = 7.5 Hz, 1H), 6.46 (d, *J* = 7.7 Hz, 2H), 5.56 (d, *J* = 8.6 Hz, 1H), 4.11 (s, 3H), 1.77 (s, 15H). Elemental analysis: Found: C, 59.51; H, 5.18; N, 4.45%, calcd for $C_{31}H_{32}ClIrN_2$: C, 59.59; H, 5.16; N, 4.48%. ESI-MS (*m/z*): calcd for $C_{31}H_{32}IrN_2$: 624.57 $[M\text{-}Cl]^+$; found 625.33.

Acknowledgments

We thank the University Research Development Program of Shandong Province (J18KA082), the National Natural Science Foundation of China (Grant No. 21671118) and the Taishan Scholars Program for support.

References

[1] L. Galluzzi, L. Senovilla, I. Vitale, J. Michels, I. Martins, O. Kepp, M. Castedo, G. Kroemer, Oncogene 31 (2011)1869-1873.

[2] C.-H. Leung, H.-J. Zhong, D.S.-H. Chan, D.-L. Ma, Coord. Chem. Rev. 257 (2013) 1764-1776.

[3] F.-X. Wang, M.-H. Chen, X.-Y. Hu, R.-R. Ye, C.-P. Tan, L.-N. Ji, Z.-W. Mao, Sci. Rep. 6 (2016) 38954.

[4] H. Zhang, L. Guo, Z. Tian, M. Tian, S. Zhang, Z. Xu, P. Gong, X. Zheng, J. Zhao, Z. Liu, Chem. Commun. 54 (2018) 4421-4424.

[5] A. Wilbuer, D.H. Vlecken, D.J. Schmitz, K. Kräling, K. Harms, C.P. Bagowski, E. Meggers, Angew. Chem. Intl. Ed. 49 (2010) 3839-3842.

[6] Y. Li, C.-P. Tan, W. Zhang, L. He, L.-N. Ji, Z.-W. Mao, Biomaterials 39 (2015) 95-104.

[7] L. Zeng, P. Gupta, Y. Chen, E. Wang, L. Ji, H. Chao, Z.-S. Chen, Chem. Soc. Rev. 46 (2017) 5771-5804.

[8] Z. Liu, P.J. Sadler, Acc. Chem. Res. 47 (2014) 1174-1185.

[9] N. Muhammad, Z. Guo, Curr. Opin. Chem. Biol. 19 (2014) 144-153.

[10] L. Feng, Y. Geisselbrecht, S. Blanck, A. Wilbuer, G.E. Atilla-Gokcumen, P. Filippakopoulos, K. Kräling, M.A. Celik, K. Harms, J. Maksimoska, R. Marmorstein, G. Frenking, S. Knapp, L.-O. Essen, E. Meggers, J. Am. Chem. Soc. 133 (2011) 5976-5986.

[11] Z. Liu, I. Romero-Canelón, B. Qamar, J.M. Hearn, A. Habtemariam, N.P.E. Barry, A.M. Pizarro, G.J. Clarkson, P.J. Sadler, Angew. Chem. Intl. Ed. 126 (2014) 4022-4027.

[12] M. Böge, C. Fowelin, P. Bednarski, J. Heck, Organometallics 34 (2015) 1507-1521.

[13] L.C. Sudding, R. Payne, P. Govender, F. Edafe, C.M. Clavel, P.J. Dyson, B. Therrien, G.S. Smith, J. Org. Chem. 774 (2014) 79-85.

[14] G.S. Yellol, A. Donaire, J.G. Yellol, V. Vasylyeva, C. Janiak, J. Ruiz, Chem. Commun. 49 (2013) 11533-11535.

[15] S. Díez-González, N. Marion, S.P. Nolan, Chem. Rev. 109 (2009) 3612-3676.

[16] B.K. Paul, N. Guchhait, Photochem. Photobiol. Sci. 10 (2011) 980-991.

[17] F. Schmitt, K. Donnelly, J.K. Muenzner, T. Rehm, V. Novohradsky, V. Brabec, J. Kasparkova, M. Albrecht, R. Schobert, T. Mueller, J. Inorg. Biochem. 163 (2016) 221-228.

[18] Z. Deng, L. Yu, W. Cao, W. Zheng, T. Chen, Chem. Commun. 51 (2015) 2637-2640.

[19] Y. Li, X. li, W. Zheng, C. Fan, Y. Zhang, T. Chen, J. Mater. Chem. 1 (2013) 6365-6372.

[20] J. Liu, Y. Chen, G. Li, P. Zhang, C. Jin, L. Zeng, L. Ji, H. Chao, Biomaterials. 56 (2015) 140-153.

[21] S. Fulda, L. Galluzzi, G. Kroemer, Nat. Rev. Drug Discovery 9 (2010) 447.

[22] R.A.J. Smith, R.C. Hartley, M.P. Murphy, Antioxid. Redox Signaling 15 (2011) 3021-3038.

[23] J. Zhu, L. Wu, Q. Zhang, X. Chen, X. Liu, Spectrochim. Acta Part A. 95 (2012) 252-257.

[24] Z. Xu, D. Kong, X. He, L. Guo, X. Ge, X. Liu, H. Zhang, J. Li, Y. Yang, Z. Liu, Inorg. Chem. Front. 2018.

[25] J.J. Soldevila-Barreda, A. Habtemariam, I. Romero-Canelón, P.J. Sadler, J. Inorg. Biochem. 153 (2015) 322-333.

[26] W. Zhang, C.-H. Tung, Chem. Eur. J. 24 (2018) 2089-2093

[27] H. Huang, L. Yang, P. Zhang, K. Qiu, J. Huang, Y. Chen, J. Diao, J. Liu, L. Ji, J. Long, H. Chao, Biomaterials. 83 (2016) 321-331.

[28] L. He, Y. Huang, H. Zhu, G. Pang, W. Zheng, Y.-S. Wong, T. Chen, Adv. Funct. Mater. 24 (2014) 2754-2763.

[29] E. Schuh, C. Pflüger, A. Citta, A. Folda, M.P. Rigobello, A. Bindoli, A. Casini, F. Mohr, J. Med. Chem. 55 (2012) 5518-5528.

[30] C. Wang, J. Liu, Z. Tian, M. Tian, L. Tian, W. Zhao, Z. Liu, Dalton. Trans. 46 (2017) 6870-6883.

[31] A. Pflug, M. Lukarska, P. Resa-Infante, S. Reich, S. Cusack, Virus. Research. 234 (2017) 103-117.

[32] Z. Liu, R.J. Deeth, J.S. Butler, A. Habtemariam, M.E. Newton, P.J. Sadler, Angew. Chem. Int. Ed. 52 (2013) 4194-4197.

[33] S. Betanzos-Lara, Z. Liu, A. Habtemariam, A.M. Pizarro, B. Qamar, P.J. Sadler, Angew. Chem. Int. Ed. 51 (2012) 3897-3900.

[34] S. Chatterjee, T.K. Mukherjee, Phys. Chem. Chem. Phys. 16 (2014) 8400-8408.

[35] E. Ramachandran, D. Senthil Raja, N.S.P. Bhuvanesh, K. Natarajan, Dalton. Trans. 41 (2012) 13308-13323.

[36] D.S. Raja, N.S.P. Bhuvanesh, K. Natarajan, Dalton. Trans. 41 (2012) 4365-4377.

[37] Z. Chen, J. Zhang, C. Liu, BioMetals. 26 (2013) 827-838.

[38] J. Fernández-Gallardo, B.T. Elie, F.J. Sulzmaier, M. Sanaú, J.W. Ramos, M. Contel, Organometallics 33 (2014) 6669-6681.

[39] H. Naz, P. Khan, M. Tarique, S. Rahman, A. Meena, S. Ahamad, S. Luqman, A. Islam, F. Ahmad, M.I. Hassan, Int. J. Biol. Macromol. 96 (2017) 161-170.

[40] N. Selvakumaran, N.S.P. Bhuvanesh, A. Endo, R. Karvembu, Polyhedron 75 (2014) 95-109.

[41] B. Buscher, S. Laakso, H. Mascher, K. Pusecker, M. Doig, L. Dillen, W. Wagner-Redeker, T. Pfeifer, P. Delrat, P. Timmerman, Bioanalysis 6 (2014) 673-682.

[42] X. He, M. Tian, X. Liu, Y. Tang, C.F. Shao, P. Gong, J. Liu, S. Zhang, L. Guo, Z. Liu, Chem Asian J. 13 (2018) 1500-1509.

[43] A. Baral, L. Satish, D.P. Das, H. Sahoo, M.K. Ghosh, New. J. Chem. 41 (2017) 8130-8139.

[44] P. Zhang, S. Zhuo, L. Sun, P. Zhang, C. Zhu, R. Soc. Chem. 39 (2015) 4551-4555.

[45] M. Polson, S. Fracasso, V. Bertolasi, M. Ravaglia, F. Scandola, Inorg. Chem. 43 (2004) 1950-1956.

[46] R. Rubbiani, S. Can, I. Kitanovic, H. Alborzinia, M. Stefanopoulou, M. Kokoschka, S. Mönchgesang, W.S. Sheldrick, S. Wölfl, I. Ott, J. Med. Chem. 54 (2011) 8646-8657.

[47] Y. Jiang, G. Liu, X. Wang, J. Hu, G. Zhang, S. Liu, Macromolecules 48 (2015) 764-774.

[48] M. Nichi, T. Rijsselaere, J.D.A. Losano, D.S.R. Angrimani, G.K.V. Kawai, I.G.F. Goovaerts, A. Van Soom, V.H. Barnabe, J.B.P. De Clercq, P.E.J. Bols, Reprod. Domest. Anim. 52 (2017) 257-263.

[49] H. Antonicka, K. Choquet, Z.Y. Lin, A.C. Gingras, C.L. Kleinman, E.A. Shoubridge, EMBO Rep. 18 (2017) 28-38.

[50] X. Wang, M. Zhu, F. Gao, W. Wei, Y. Qian, H.-K. Liu, J. Zhao, J. Inorg. Biochem. 180 (2018) 179-185.

[51] S. Daum, M.S.V. Reshetnikov, M. Sisa, T. Dumych, M.D. Lootsik, R. Bilyy, E. Bila, C. Janko, C. Alexiou, M. Herrmann, L. Sellner, A. Mokhir, Angew. Chem. Int. Ed. 56 (2017) 15545-15549.

[52] L. He, C.P. Tan, R.R. Ye, Y.Z. Zhao, Y.H. Liu, Q. Zhao, L.N. Ji, Z.W. Mao, Angew. Chem. Int. Ed. 53 (2014) 12137-12141.

[53] C. Li, M. Yu, Y. Sun, Y. Wu, C. Huang, F. Li, J. Am. Chem. Soc. 133 (2011) 11231-11239.

[54] Z. Liu, A. Habtemariam, A.M. Pizarro, S.A. Fletcher, A. Kisova, O. Vrana, L. Salassa, P.C.A. Bruijnincx, G.J. Clarkson, V. Brabec, P.J. Sadler, J.Med. Chem. 54 (2011) 3011-3026.

Graphical Abstracts

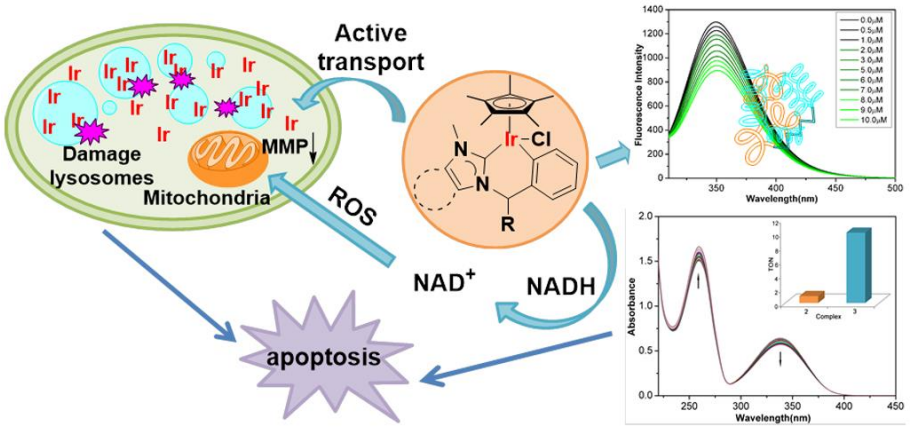

Ir^{III} *N*-heterocyclic carbene complexes can catalyze nicotinamide adenine dinucleotide (NADH) to NAD^+, induce reactive oxygen species (ROS), bonding to bovine serum albumin (BSA) and reduce the mitochondrial membrane potential (MMP). Complexes could target lysosome, and through energy-dependent cellular uptake mechanism.

Highlights

1. Ir^{III} complexes showed potent antitumor activity against A549 cells than cisplatin.
2. Ir^{III} complexes could target the lysosome and mitochondria in tumor cells.
3. Ir^{III} complexes enter cells followed by an energy-dependent cellular uptake mechanism.